

Evidence of indium impurity band in superconducting (Sn,In)Te thin films

Jiashu Wang ¹, Trisha Musall ¹, Bo-An Chen,^{2,3} Marie Gerges,¹ Logan Riney,¹
Sylwia Ptasińska,^{1,2} Xinyu Liu,¹ and Badih A. Assaf ¹

¹*Department of Physics and Astronomy, University of Notre Dame, Notre Dame, Indiana 46556, USA*

²*Radiation Laboratory, University of Notre Dame, Notre Dame, Indiana 46556, USA*

³*Department of Chemistry and Biochemistry, University of Notre Dame, Notre Dame, Indiana 46556, USA*



(Received 11 October 2023; revised 20 November 2023; accepted 20 December 2023; published 16 January 2024)

$\text{Sn}_{1-x}\text{In}_x\text{Te}$ has been synthesized and studied recently as a candidate topological superconductor. Its superconducting critical temperature increases with indium concentration. However, the role of indium in altering the normal-state band structure and generating superconductivity is not well understood. Here, we explore this question in $\text{Sn}_{1-x}\text{In}_x\text{Te}$ ($0 < x < 0.3$) thin films, characterized by magnetotransport, infrared transmission, and photoemission spectroscopy measurement. We show that indium is forming an impurity band below the valence-band edge which pins the Fermi energy and effectively generates electron doping. An enhanced density of states due to this impurity band leads to the enhancement of T_c measured in multiple previous studies. The existence of the In impurity band and the role of In as a resonant impurity should be more carefully considered when discussing the topological nature of $\text{Sn}_{1-x}\text{In}_x\text{Te}$.

DOI: [10.1103/PhysRevB.109.014513](https://doi.org/10.1103/PhysRevB.109.014513)

I. INTRODUCTION

Topological superconductors (TSCs) have a superconducting gap in the bulk with gapless boundary states. They not only enrich scientists' understanding of topological phases, but also have promising applications [1–3]. Chiral p -wave topological superconductors, for example, are potential platforms for topological quantum computing [4]. These materials are rare in nature. There are ongoing efforts to artificially engineer topological superconductors using semiconductor-superconductor heterostructures [5]. Other ongoing efforts also aim to find intrinsic topological superconductors. In the recent decade, the following candidate materials were proposed as potential TSCs: $\text{Cu}_x\text{Bi}_2\text{Se}_3$ [6,7], UTe_2 [8], UPt_3 [9], and $\text{Sn}_{1-x}\text{In}_x\text{Te}$ [10,11].

SnTe is a topological crystalline insulator [12,13]. It hosts four Dirac cones protected by mirror symmetry on its (111) and (100) surfaces. Through indium doping, it becomes superconducting without losing its topological properties [10,14]. It is a TSC candidate, since its superconducting state can be described by the Hamiltonian proposed by Fu and Berg [6,10] to predict the TSC state in $\text{Cu}_x\text{Bi}_2\text{Se}_3$ [11]. The $\text{Cu}_x\text{Bi}_2\text{Se}_3$ material family has been well studied experimentally. There, Cu intercalates between the Se layers and acts as an electron donor. Its role in generating superconductivity is understood [7,15]. The pairing symmetry in $\text{Sn}_{1-x}\text{In}_x\text{Te}$ remains controversial [16–18], but recent work has shown it is dominantly s wave [19] at high In content, despite previous work arguing that surface states persist in the superconducting state [16]. The role of In in $\text{Sn}_{1-x}\text{In}_x\text{Te}$ still lacks sufficient understanding. In is usually considered an acceptor in IV–VI materials [14], but prior studies on single crystals have argued that In actually forms an impurity band near the Fermi level and acts effectively as a donor [20–22]. One manifestation of the impurity band in these studies was the reduction of the Hall

constant, associated with coexisting electrons and holes. A spectroscopic measurement is needed to probe the band structure and to provide evidence of the existence of the impurity band.

Here, we analyzed the role of In in $\text{Sn}_{1-x}\text{In}_x\text{Te}$ thin films by a combination of magnetotransport, infrared spectroscopy measurements, and x-ray photoelectron spectroscopy. Magnetotransport measurements show that the Hall slope of $\text{Sn}_{1-x}\text{In}_x\text{Te}$ films becomes 100 times smaller with increasing In concentration and increasing T_c , consistent with prior work on single crystals. The calculated carrier density is however unreasonably high, indicating a likely existence of both electrons and holes. We consider the impurity-band model to explain this observation, and we corroborate the model using optical measurements of the absorption edge that evidence a pinning of the Fermi energy in the valence band. Last, x-ray and ultraviolet photoemission spectroscopy (XPS and UPS, respectively) measurements confirm that In is indeed a resonant impurity and introduces a band below the valence-band edge of SnTe . Our studies show that pairing involving indium impurity states should be taken into consideration carefully when discussing the topological properties of $\text{Sn}_{1-x}\text{In}_x\text{Te}$, especially at high In content needed to enhance T_c above 2 K.

II. EXPERIMENTS**A. Sample growth**

Superconducting $\text{Sn}_{1-x}\text{In}_x\text{Te}$ films on BaF_2 (111) substrates with controlled indium concentration ($x = 0–0.3$) are grown by molecular-beam epitaxy. A 25-nm SnTe layer is grown first, followed by a 75-nm $\text{Sn}_{1-x}\text{In}_x\text{Te}$ layer. We find that the indium diffuses fully into the SnTe layer, thus forming a uniform 100-nm $\text{Sn}_{1-x}\text{In}_x\text{Te}$ single layer [Fig. 1(a)]. X-ray diffraction (XRD) analysis published in our previous work

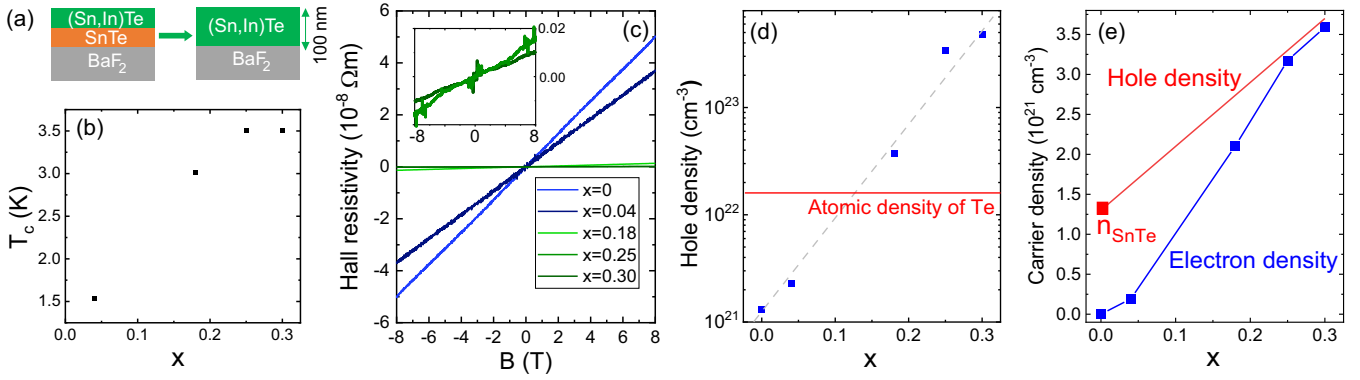


FIG. 1. (a) Sample structure: 25-nm SnTe and 75-nm $\text{Sn}_{1-x}\text{In}_x\text{Te}$ are grown in sequence on BaF_2 (111) substrate. In diffuses into the SnTe layer, resulting in a uniform $\text{Sn}_{1-x}\text{In}_x\text{Te}$ layer. (b) Critical superconducting temperature T_c of samples with different In content x . (c) Hall resistivity of samples with different In content x . Inset: Zoom-in image of the Hall resistivity for $x = 0.25$ and $x = 0.3$. (d) Extracted carrier density, assuming a single-carrier type (p type). The gray dashed line is a guide for the eye. The red line is the calculated atomic density of Te, assuming the lattice constant is 6.3 \AA . (e) Extracted electron density with two-carrier model assuming electrons and holes with similar mobility coexist and hole density increases linearly with In concentration x . The red dot is the experimental data of pure SnTe film.

showed the sample has a rocksalt structure, with slight compressive in-plane strain and tensile strain in the out-of-plane direction. The In concentration, sample thickness, and strain were confirmed by XRD, transmission electron microscopy, and energy-dispersive spectroscopy (EDS). The characterization results are shown in Ref. [23].

B. Magnetotransport measurements

Electrical magnetotransport measurements are performed between 1.5 and 15 K in a custom system equipped with a standard superconducting coil, covering both the superconducting and normal state. The critical superconducting temperature T_c increases with x , and can reach 3.5 K with $x = 0.3$ [Fig. 1(b)]. The order of magnitude of T_c is consistent with previous work on thin films of (Sn,In)Te [24,25]. The superconducting properties, as well as the longitudinal magnetoresistance in the normal state, are discussed in detail in Ref. [23]. Here, we will focus on the Hall effect and optical properties of $\text{Sn}_{1-x}\text{In}_x\text{Te}$ in the normal state, as they tightly relate to the role of the In impurity.

The Hall resistivity of our $\text{Sn}_{1-x}\text{In}_x\text{Te}$ films at 6 K is shown in Fig. 1(c). All samples exhibit a p -type behavior with a constant Hall slope. As x increases, the Hall slope decreases dramatically. Particularly, for samples with $x = 0.25$ and $x = 0.3$, the Hall slope is two orders smaller than for those with lower x [Fig. 1(c), inset]. If we assume that In is providing acceptors and generating holes, the hole density can be calculated from the Hall slope. It is shown as blue dots in Fig. 1(d). With this assumption, we recover unreasonably large hole densities for high x . From the average lattice constant 6.3 \AA , the Te atomic density is around $1.6 \times 10^{22} \text{ cm}^{-3}$, indicated by the red line in Fig. 1(d). Hole densities for $x > 0.18$ exceed this limit by more than an order of magnitude.

The most plausible explanation of this result is that a portion of In actually acts as electron donors (In^{3+}). Meanwhile, the remaining In (In^{1+}) as well as Sn vacancies act as acceptors providing holes. The system then hosts coexisting electrons and holes with comparable mobilities. Under

such conditions, the Hall resistivity in the Drude model follows

$$\rho_{xy} \approx \frac{n_h - n_e}{e(n_h + n_e)^2} B, \quad (1)$$

where $n_{h,e}$ is the carrier density of holes and electrons. The above equation holds when their mobilities are almost equal, $\mu_h \approx \mu_e$. Such an approximation is based on two experimental facts: (1) The Hall slope remains perfectly linear at all indium concentrations, which indicates carriers having a similar mobility; and (2) The hole mobility of pure SnTe ($x < 0.01$) grown for this work is already quite low (10 to $59 \text{ cm}^2/\text{V s}$). Thus, when the electron density is close to the hole density, the slope of the Hall resistivity is reduced, resulting in an abnormally large density of “single carriers.” We note that in Ref. [20], the authors made a similar observation but fit their Hall measurements by considering a changing mobility of localized electrons. Since there are more fitting parameters than constraints in this model, both our conclusions are similar in reflecting the role of electrons in transport. n_e can be viewed as a density of “effective free electrons” with mobility equal to that of holes.

Under these assumptions, we can utilize the hole density n_0 of pure SnTe ($x = 0$) to approximate the electron density of other samples. We assume an approximation that the hole density increases linearly with In concentration:

$$n_h = n_{\text{SnTe}} + \frac{x}{2} n_0,$$

where n_{SnTe} is the measured hole density of pure SnTe film and n_0 is the atomic density of Te. The approximation here is assuming half the indium acts like In^{1+} and donates holes and the other half acts like In^{3+} and donates electrons. The calculated n_e (effective free electrons) is not necessarily equal to the density of In^{3+} since a portion of the impurity carriers may be localized. n_h is taken into Eq. (1) to calculate n_e . The result is shown in Fig. 1(e). As the In concentration rises, more electrons contribute to the transport, causing the Hall slope to decrease dramatically.

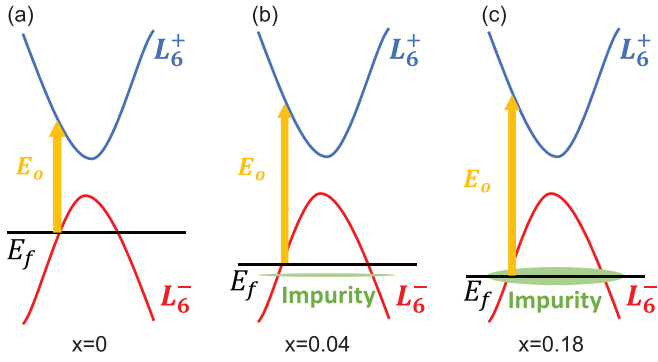


FIG. 2. Evolution of the band structure with increasing In concentration x . (a) $x = 0$, Fermi level E_f lies below the valence-band edge. Yellow arrow indicates the energy of the optical transition (optical gap E_o) from the conduction band to the valence band. (b) $x = 0.04$; E_f moves further down, and an indium impurity band forms (green). (c) $x = 0.18$; E_f reaches the impurity-band region and gets pinned to it. L_6^\pm denote the conduction- and valence-band edges of SnTe at the L points of the Brillouin zone.

Previous studies have also suggested that as the In concentration gets higher, In $5s$ and Te $5p$ orbitals hybridize and form an impurity band below the Fermi level E_f [21]. This, together with the transport analysis, leads us to a physical picture as shown in Fig. 2. With small x , most indium atoms are In^+ and thus donate holes to the system, bringing E_f further down into the valence band as indicated by the decreasing Hall slope. When the In concentration becomes large enough, an In $5s$ -Te $5p$ hybridized impurity band forms and pins the E_f to its position. The impurity band donates electrons to the system.

C. Optical infrared spectroscopy

The above scenario is based on magnetotransport measurements and follows what was hypothesized in previous studies using density-functional theory (DFT) calculations [21]. To validate such a model, we additionally perform Fourier-transform infrared (FTIR) transmission spectroscopy at room temperature in a Bruker Vertex 80v setup equipped with a CaF_2 beam splitter for the near infrared to reach 15000 cm^{-1} . Our thin films enable measurements in the transmission geometry not possible on thick conducting crystals. By dividing the transmitted intensity through the samples (T_{sample}) by that measured through a pure BaF_2 substrate (T_{sub}), we can get the relative transmission signal through each film. The results are shown in Fig. 3(a). A wide transparency region is seen in the midinfrared well into the near infrared for most samples, consistent with $\text{Sn}_{1-x}\text{In}_x\text{Te}$ retaining a semiconducting normal state. A sudden drop in the intensity indicates a corresponding optical interband transition with energy equal to the photon energy $h\nu$. It is plotted as the yellow arrow E_o in Fig. 2. The position of this transmission edge blueshifts with increasing x , indicating an increasing optical gap. The detection of E_o is important as it directly probes the position of the Fermi level E_f . That is because $\text{Sn}_{1-x}\text{In}_x\text{Te}$ is degenerately doped, which Pauli blocks band-edge to band-edge transitions. The measured optical gap will then include the Moss-Burstein

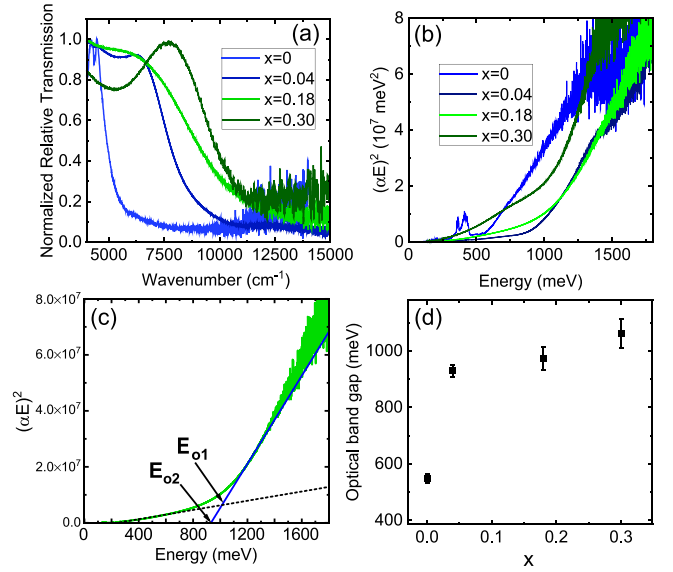


FIG. 3. FTIR transmission spectroscopy for $\text{Sn}_{1-x}\text{In}_x\text{Te}$ films with different x . (a) Relative transmission intensity of samples in the midinfrared and near-infrared range. The drop indicates the absorption caused by interband optic transitions. (b) Tauc plot of the data shown in (a). (c) Extraction of the optical gap E_o from the Tauc plot shown for $x = 0.18$. The blue is a linear fit of the absorption edge, and the dashed black line is a linear fit of the background. Two values of E_o are determined from the intercept of the blue line with the x -axis E_{o2} and with the background E_{o1} . The average of the two is reported and their standard deviation is taken as the uncertainty on E_o . (d) Extracted optical gap E_o of the four samples vs x .

shift and is given by $E_o = E_g + 2E_f$, assuming electron-hole symmetry.

A more accurate estimation of E_o is to use the Tauc plot method, expressed by the equation [26]

$$(\alpha h\nu)^{1/\gamma} = B(h\nu - E_o).$$

Here, $\alpha = -\ln(T_{\text{sample}}/T_{\text{sub}})$ is the absorption coefficient, $\gamma = 1/2$ for direct band transition. By this equation, it becomes more convenient to rearrange the data to a Tauc plot in Fig. 3(b). The intercept between the rising linear absorption edge in the Tauc plot and the x axis is the value of the optic gap, as illustrated by E_{o2} in Fig. 3(c). Since our baseline is not perfectly flat, we can also extract the optical gap as the point of intercept with an energy-dependent baseline, as indicated by E_{o1} in Fig. 3(c). Thus, to include the effect of uncertainty from the background, an average of E_o along an error can be extracted for all samples from the two values $E_{o1,o2}$.

The results of E_o as a function of composition x are shown in Fig. 3(d). The optical gap of SnTe is found to be 550 meV. If we take the direct fundamental band gap of SnTe to be $E_g = 0.18 \text{ eV}$ [27,28], this yields a Fermi level of 175 meV below the valence-band edge without In. The qualitative behavior of the optical gap with increasing In content is important to highlight. It increases to 930 meV for $x = 0.04$, but rises more slowly between $x = 0.04$ and $x = 0.30$, despite the Hall voltage dropping by two orders of magnitude. This is consistent with a pinning of E_f attributed to the emergence of an impurity band.

The trend of optical gap with x agrees with the proposed model in Fig. 2. The value of the optical gap E_o directly reflects the position of the Fermi level. Larger E_o implies E_f lies deeper in the valence band. At small x , In mostly gives holes to the system, leading to a fast drop of the Fermi level compared to SnTe. At $x > 0.04$, an impurity band forms and E_f gets pinned at its position. E_o then remains relatively unchanged. If we assume that (Sn,In)Te also has a direct band gap E_g of 0.18 eV at room temperature, this indicates that the impurity band lies around 400 meV below the valence-band edge.

It is worth noting here that in SnTe, a heavy-hole band lying 0.3–0.5 eV below the valence-band edge has been identified in the past [29,30]. It is referred to as the Σ band. It needs to be ruled out as possible source of Fermi-level pinning that can explain the flat trend of E_o upon introduction of indium. If E_f crosses the Σ band, the density of states at E_f becomes larger and requires more holes to lower E_f . However, the slope of E_o vs x in Fig. 3(d) is extremely small and does not exceed 5 meV/1%. Additionally, the behavior of the Hall voltage, dropping by almost an order of magnitude, cannot be accounted for by the Σ band. Additionally, taking the heavy-hole effective mass to be $m_\Sigma \approx 2m_0$ [29,30], we can compute the hole density supported by this band as a function of energy assuming a simple spherical Fermi surface. This assumption will overestimate the carrier density. We find that E_f needs to be more than 1.5 eV below the Σ band to get a carrier density that exceeds 10^{23}cm^{-3} , which is not consistent with the pinning of E_f . Hence, the density of states of the heavy-hole Σ band is not sufficiently high to account for our measured Hall density. In Ref. [23] we showed that the lattice constant of $\text{Sn}_{1-x}\text{In}_x\text{Te}$ decreases linearly with x . From $x = 0$ to $x = 0.30$ the lattice constant changes quasilinearly from 6.33 to 6.27 Å. Thus, it is necessary to consider the role of strain on the band gap. If we view it as an effective compressive strain to the SnTe lattice, the modification to the band gap can be calculated using

$$\Delta E_g = D_d(2\varepsilon_{\parallel} + \varepsilon_{\perp}) + D_u(8\varepsilon_{\parallel} + \varepsilon_{\perp})/9,$$

where $\varepsilon = \frac{a}{a_0} - 1$ and $D_{d,u}$ are deformation potentials which can be found in Ref. [31]. Here, we are neglecting the strain coming from the BaF_2 substrate and assume the $x = 0$ lattice constant is the relaxed a_0 . Then, we get that the band-gap modification is negligible for $x = 0.04$; 29 meV for $x = 0.18$; and 35 meV for $x = 0.30$. Thus, strain can increase the band gap by no more than 35 meV, which can partially explain the increase of the optical gap in the $x > 0.04$ region but cannot explain the strong enhancement of E_o from $x = 0$ to $x = 0.04$.

The optical measurements shown in Fig. 3 were all carried out at room temperature, but we also performed low-temperature FTIR measurements down to 4.2 K (see Appendix A). As E_f drops with temperature, E_o also drops. But, sample-to-sample variations due to the changing chemical composition remain much larger than the slight temperature dependence of the gap. We conclude that the discussion of optical measurements at room temperature also applies at low temperature to the normal state of the system right before it goes to superconducting.

D. X-ray- and ultraviolet photoemission spectroscopies

Next, photoelectron spectroscopic measurements are performed using a system which combines two photoemission sources: x rays and ultraviolet light, purchased from SPECS Surface Nano Analysis GmbH (Berlin, Germany). XPS spectra were recorded using a monochromatized Al $K\alpha$ (1486.7 eV) x-ray beam generated by a microfocus x-ray source, while UPS spectra were recorded using He I (21.2 eV) generated by a plasma excitation source. The details of this experimental system were described previously [32]. The details of the sample preparation are discussed in Appendix B.

UPS data, shown in Fig. 4(a), further reveal the changing shape of the valence band upon introduction of In. Slightly below the Fermi energy, marked by a black arrow, a peak is observed for both $x = 0.04$ and $x = 0.3$. The peak does not shift in energy, but the intensity becomes stronger with In concentration. Such behavior indicates an enhanced density of states in the valence band of $\text{Sn}_{1-x}\text{In}_x\text{Te}$, consistent with the impurity-band picture. The results of UPS imply that the increasing In leads to the formation of an impurity band below the valence-band edge likely due to the In 5s-Te 5p hybridization.

Last, to further elucidate the mixed valence of indium needed to explain the Hall effect, we performed XPS on the $x = 0.04, 0.18$, and 0.30 samples [Figs. 4(b)–4(d)]. All XPS spectra are calibrated using the Sn $3d_{5/2}$ peak at a binding energy of 485.2 eV [33]. The Sn $3d$ XPS peaks are shown in Fig. 4(c). The Te $3d$ peaks [Fig. 4(b)] do not exhibit any dramatic changes with increasing In content. The In $3d$ peaks are shown in Fig. 4(d) and analyzed in detail in Appendix B. We notice that the peak position is almost independent of x (within 0.1 eV) from $x = 0.04$ to $x = 0.30$. However, the In $3d$ peaks become more asymmetric with increasing x , indicating the likely presence of a second peak on the high-energy tail of the main one [Fig. 4(d)]. In is known to skip the 2+ valence [34] and has been hypothesized to have mixed (+1 and +3) valence in $\text{Sn}_{1-x}\text{In}_x\text{Te}$, similar to Tl in PbTe [35,36]. We cannot however distinguish the two components and attribute them to specific oxidation states, as their peak values are closer to each other than what is expected for In^{+3} and In^+ [37]. However, the proximity of the In^+ and In^{3+} XPS peaks makes it challenging to fit spectra and to confirm their mixed-valence character (see Appendix B). It is also possible that the high-energy peak is due to a strong In 5s – Te5p hybridization reported in DFT calculations [21].

III. CONCLUSION

In summary, magnetotransport, optical absorption, and photoemission spectroscopy measurements corroborate the presence of an In impurity band in $\text{Sn}_{1-x}\text{In}_x\text{Te}$ thin films. Experimentally, a dramatic decrease of the Hall slope with increasing In concentration x is observed, while optical measurements reveal a weakly varying optical gap for $x \geq 0.04$. These observations indicate that the Fermi level is pinned to an impurity band. The hypothesis is further supported by UPS measurements, which show the changing shape of the valence band. While XPS measurements could not conclusively differentiate specific oxidation states of In, they did reveal

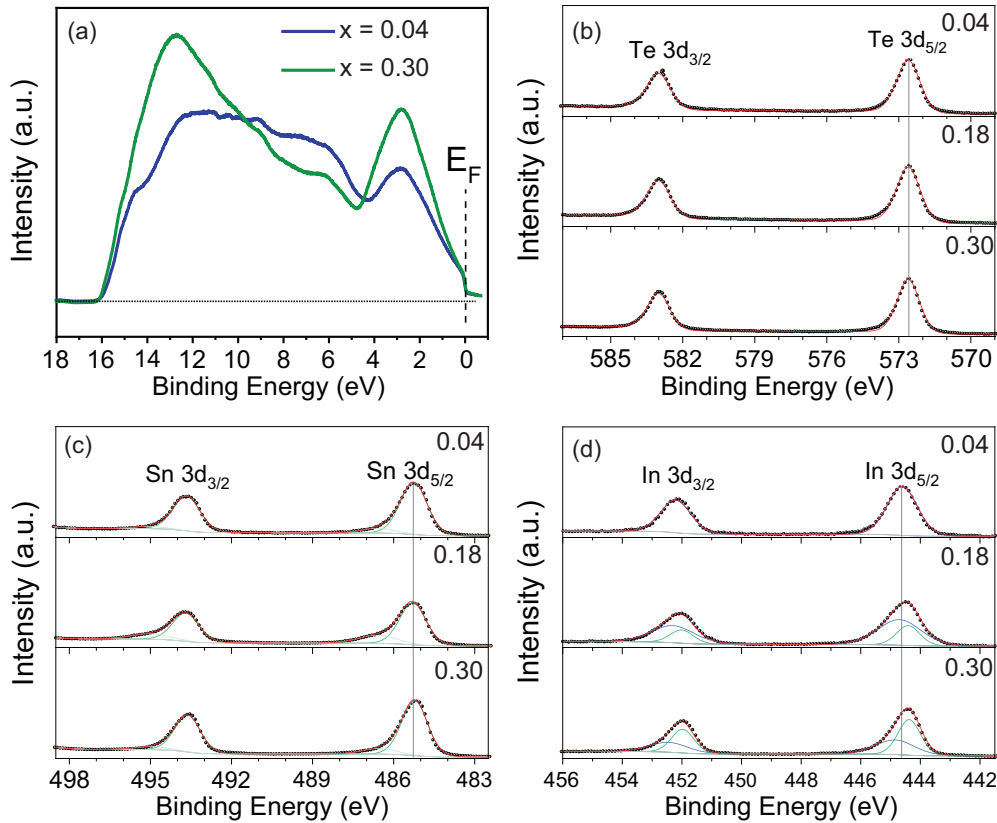


FIG. 4. (a) UPS spectra of $\text{Sn}_{1-x}\text{In}_x\text{Te}$ films with $x = 0.04$ and 0.30 . XPS spectra of the Te $3d$ (b), Sn $3d$ (c), and In $3d$ (d) peaks for $x = 0.04, 0.18,$ and 0.30 . The Sn spectra are used for calibration of the binding energy. The black dots represent data points and the solid red lines represent the overall fit to the data. The green and blue lines represent individual peaks included in the fit.

an asymmetric In peak at high In content. This is consistent with the mixed-valence picture, but could also originate from a hybridization of the In and Te levels. Since $\text{Sn}_{1-x}\text{In}_x\text{Te}$ is commonly viewed as a potential topological superconductor, the existence of the In impurity band should be more carefully considered when discussing its topological nature. Prior work hypothesizing topological superconductivity has essentially considered pairing near the valence-band edge for this material, involving Sn and Te orbitals of opposite parity [11]. However, the experimental results shown here, as well as prior measurements on single crystals consistent with our interpretation, indicate that such a treatment is not sufficient to understand the nature of superconductivity in this material [21,23,38,39]. At the very least, proper models of the superconductivity of $\text{Sn}_{1-x}\text{In}_x\text{Te}$ must take into account the changing band structure of this material's valence band upon introduction of In.

ACKNOWLEDGMENTS

This work was supported by National Science Foundation Award No. DMR-1905277. T.M. also acknowledges support from the Notre Dame REU program through National Science Foundation Award No. PHY-2050527. B.-A.C. and S.P. acknowledge support from the U.S. Department of Energy Office of Science, Office of Basic Energy Sciences under Award No. DE-FC02-04ER15533 (NDRL 5418). L.R. was partly

supported by Civilian Research and Development Foundation Global Grant No. G-202206-6887.

APPENDIX A: LOW-TEMPERATURE OPTICAL TRANSMISSION SPECTROSCOPY

The optical transmission spectroscopy measurements discussed in the main text are repeated at low temperature, down to 4.2 K. The variation of the optical gap versus temperature

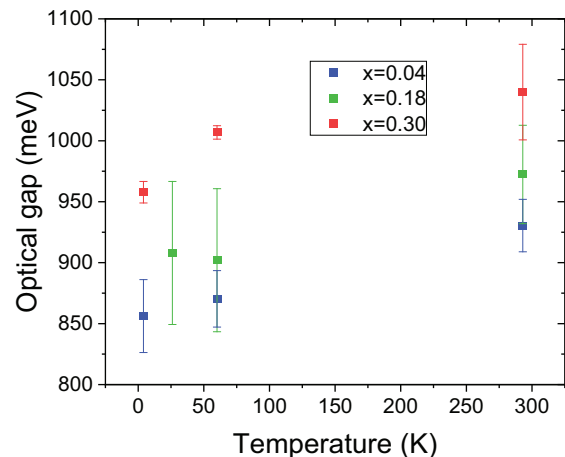


FIG. 5. Temperature dependence of the optical band gap in $\text{Sn}_{1-x}\text{In}_x\text{Te}$ films.

TABLE I. XPS spectra fitting results for the curves shown in Fig. 4(d).

	$x = 0.04$	$x = 0.18$		$x = 0.30$		InI	InI ₂	InI ₃
Binding energy (eV)	444.6	444.7	444.4	444.8	444.4	444.0	445.1	445.1
FWHM ^a (eV)	1.18	1.7	0.91	1.53	0.88			
Weight	1	0.70	0.30	0.42	0.58			
Reference		This work Sn _{1-x} In _x Te					[40]	

^aFull width at half maximum.

is shown in Fig. 5. It is evident that the sample-to-sample variations seen at room temperature remain valid at low temperature.

APPENDIX B: ANALYSIS OF THE XPS SPECTRA

XPS measurements are carried out on Sn_{1-x}In_xTe with $x = 0.04, 0.18,$ and $0.3,$ after removal of an oxide layer by Ar⁺ ion sputtering. The presence of the oxide layer is monitored by measuring the O 1s, Sn 3d, and Te 3d signal (4+ oxidation of Te and Sn appears due to SnO₂ and TeO₂). Sputtering is carried out until we can no longer detect those specific signals. The results shown in Fig. 4 are obtained after the removal of the oxide.

A GL(30) line-shape function (70% Gaussian and 30% Lorentzian) is employed to fit individual peaks and a Shirley-type background is defined. The results for Sn and Te, respectively, confirm the 2+ and 2- oxidation expected for the two elements. The fitting results obtained for the In 3d_{5/2} peak are shown in Table I.

Sample-to-sample variations in the binding energies do not exceed 0.3 eV. The shoulder that accounts for the peak asymmetry for $x = 0.18$ and $x = 0.3$ in Fig. 4(d) yields a peak that is at most 0.4 eV off the main peak. These variations are smaller than variations seen in the In 3d_{5/2} peak as the oxidation state changes from 1+ (InI) to 3+ (InI₃). The table shows this comparison for iodides as a reference that this holds for other binary In compounds [37,40].

- [1] X.-L. Qi and S.-C. Zhang, Topological insulators and superconductors, *Rev. Mod. Phys.* **83**, 1057 (2011).
- [2] X. L. Qi, T. L. Hughes, S. Raghu, and S. C. Zhang, Time-reversal-invariant topological superconductors and superfluids in two and three dimensions, *Phys. Rev. Lett.* **102**, 187001 (2009).
- [3] M. Sato and Y. Ando, Topological superconductors: A review, *Rep. Prog. Phys.* **80**, 076501 (2017).
- [4] S. Das Sarma, M. Freedman, and C. Nayak, Majorana zero modes and topological quantum computation, *npj Quantum Inf* **1**, 15001 (2015).
- [5] L. Fu and C. L. Kane, Superconducting proximity effect and Majorana fermions at the surface of a topological insulator, *Phys. Rev. Lett.* **100**, 096407 (2008).
- [6] L. Fu and E. Berg, Odd-parity topological superconductors: Theory and application to Cu_xBi₂Se₃, *Phys. Rev. Lett.* **105**, 097001 (2010).
- [7] Y. S. Hor, A. J. Williams, J. G. Checkelsky, P. Roushan, J. Seo, Q. Xu, H. W. Zandbergen, A. Yazdani, N. P. Ong, and R. J. Cava, Superconductivity in Cu_xBi₂Se₃ and its implications for pairing in the undoped topological insulator, *Phys. Rev. Lett.* **104**, 057001 (2010).
- [8] S. Ran, C. Eckberg, Q.-P. Ding, Y. Furukawa, T. Metz, S. R. Saha, I.-L. Liu, M. Zic, H. Kim, J. Paglione, and N. P. Butch, Nearly ferromagnetic spin-triplet superconductivity, *Science* **365**, 684 (2019).
- [9] K. E. Avers, W. J. Gannon, S. J. Kuhn, W. P. Halperin, J. A. Sauls, L. DeBeer-Schmitt, C. D. Dewhurst, J. Gavilano, G. Nagy, U. Gasser, and M. R. Eskildsen, Broken time-reversal symmetry in the topological superconductor UPT₃, *Nat. Phys.* **16**, 531 (2020).
- [10] Y. Ando and L. Fu, Topological crystalline insulators and topological superconductors: From concepts to materials, *Annu. Rev. Condens. Matter Phys.* **6**, 361 (2015).
- [11] S. Sasaki, Z. Ren, A. A. Taskin, K. Segawa, L. Fu, and Y. Ando, Odd-parity pairing and topological superconductivity in a strongly spin-orbit coupled semiconductor, *Phys. Rev. Lett.* **109**, 217004 (2012).
- [12] L. Fu, Topological crystalline insulators, *Phys. Rev. Lett.* **106**, 106802 (2011).
- [13] T. H. Hsieh, H. Lin, J. Liu, W. Duan, A. Bansil, and L. Fu, Topological crystalline insulators in the SnTe material class, *Nat. Commun.* **3**, 982 (2012).
- [14] M. Novak, S. Sasaki, M. Kriener, K. Segawa, and Y. Ando, Unusual nature of fully gapped superconductivity in In-doped SnTe, *Phys. Rev. B* **88**, 140502(R) (2013).
- [15] P. M. R. Brydon, S. Das Sarma, H.-Y. Hui, and J. D. Sau, Odd-parity superconductivity from phonon-mediated pairing: Application to Cu_xBi₂Se₃, *Phys. Rev. B* **90**, 184512 (2014).
- [16] C. M. Polley, V. Jovic, T.-Y. Su, M. Saghir, D. Newby, Jr., B. J. Kowalski, R. Jakiela, A. Barcz, M. Guzewicz, T. Balasubramanian *et al.*, Observation of surface states on heavily indium-doped SnTe(111), a superconducting topological crystalline insulator, *Phys. Rev. B* **93**, 075132 (2016).
- [17] G. Balakrishnan, L. Bawden, S. Cavendish, and M. R. Lees, Superconducting properties of the In-substituted topological crystalline insulator SnTe, *Phys. Rev. B* **87**, 140507 (2013).
- [18] M. P. Smylie, H. Claus, W.-K. Kwok, E. R. Loudon, M. R. Eskildsen, A. S. Sefat, R. D. Zhong, J. Schneeloch, G. D. Gu, E. Bokari *et al.*, Superconductivity, pairing symmetry, and disorder in the doped topological insulator Sn_{1-x}In_xTe for $x \geq 0.1$, *Phys. Rev. B* **97**, 024511 (2018).

- [19] T. Nomoto, M. Kawamura, T. Koretsune, R. Arita, T. Machida, T. Hanaguri, M. Kriener, Y. Taguchi, and Y. Tokura, Microscopic characterization of the superconducting gap function in $\text{Sn}_{1-x}\text{In}_x\text{Te}$, *Phys. Rev. B* **101**, 014505 (2020).
- [20] C. Zhang, X.-G. He, H. Chi, R. Zhong, W. Ku, G. Gu, J. M. Tranquada, and Q. Li, Electron and hole contributions to normal-state transport in the superconducting system $\text{Sn}_{1-x}\text{In}_x\text{Te}$, *Phys. Rev. B* **98**, 054503 (2018).
- [21] N. Haldolaarachchige, Q. Gibson, W. Xie, M. B. Nielsen, S. Kushwaha, and R. J. Cava, Anomalous composition dependence of the superconductivity in in-doped SnTe, *Phys. Rev. B* **93**, 024520 (2016).
- [22] A. S. Erickson, J.-H. Chu, M. F. Toney, T. H. Geballe, and I. R. Fisher, Enhanced superconducting pairing interaction in indium-doped tin telluride, *Phys. Rev. B* **79**, 024520 (2009).
- [23] J. Wang, W. Powers, Z. Zhang, M. Smith, B. J. McIntosh, S. K. Bac, L. Riney, M. Zhukovskiy, T. Orlova, L. P. Rokhinson *et al.*, Observation of coexisting weak localization and superconducting fluctuations in strained $\text{Sn}_{1-x}\text{In}_x\text{Te}$ thin films, *Nano Lett.* **22**, 792 (2022).
- [24] W. Si, C. Zhang, L. Wu, T. Ozaki, G. Gu, and Q. Li, Superconducting thin films of (100) and (111) oriented indium doped topological crystalline insulator SnTe, *Appl. Phys. Lett.* **107**, 092601 (2015).
- [25] M. Masuko, R. Yoshimi, A. Tsukazaki, M. Kawamura, K. S. Takahashi, M. Kawasaki, and Y. Tokura, Molecular beam epitaxy of superconducting $\text{Sn}_{1-x}\text{In}_x\text{Te}$ thin films, *Phys. Rev. Mater.* **4**, 091202 (2020).
- [26] P. Makuła, M. Pacia, and W. Macyk, How to correctly determine the band gap energy of modified semiconductor photocatalysts based on UV-Vis spectra, *J. Phys. Chem. Lett.* **9**, 6814 (2018).
- [27] H. Preier, Recent advances in lead-chalcogenide diode lasers, *Appl. Phys.* **20**, 189 (1979).
- [28] S. Rabii, Energy-band structure and electronic properties of SnTe, *Phys. Rev.* **182**, 821 (1969).
- [29] T. C. Chasapis, Y. Lee, E. Hatzikraniotis, K. M. Paraskevopoulos, H. Chi, C. Uher, and M. G. Kanatzidis, Understanding the role and interplay of heavy-hole and light-hole valence bands in the thermoelectric properties of PbSe, *Phys. Rev. B* **91**, 085207 (2015).
- [30] J. He, X. Tan, J. Xu, G.-Q. Liu, H. Shao, Y. Fu, X. Wang, Z. Liu, J. Xu, H. Jiang, and J. Jiang, Valence band engineering and thermoelectric performance optimization in SnTe by Mn-alloying via a zone-melting method, *J. Mater. Chem. A Mater.* **3**, 19974 (2015).
- [31] I. I. Zasavitskii, E. A. de Andrada e Silva, E. Abramof, and P. J. McCann, Optical deformation potentials for PbSe and PbTe, *Phys. Rev. B* **70**, 115302 (2004).
- [32] X. Zhang and S. Ptasinska, Dissociative adsorption of water on an $\text{H}_2\text{O}/\text{GaAs}(100)$ interface: *In situ* near-ambient pressure XPS studies, *J. Phys. Chem. C* **118**, 4259 (2014).
- [33] V. S. Neudachina, T. B. Shatalova, V. I. Shtanov, L. V. Yashina, T. S. Zyubina, M. E. Tamm, and S. P. Kobeleva, XPS study of SnTe(100) oxidation by molecular oxygen, *Surf. Sci.* **584**, 77 (2005).
- [34] C. M. Varma, Missing valence states, diamagnetic insulators, and superconductors, *Phys. Rev. Lett.* **61**, 2713 (1988).
- [35] P. Walmsley, C. Liu, A. D. Palczewski, P. Giraldo-Gallo, C. G. Olson, I. R. Fisher, and A. Kaminski, Direct spectroscopic evidence for mixed-valence TI in the low carrier-density superconductor $\text{Pb}_{1-x}\text{Ti}_x\text{Te}$, *Phys. Rev. B* **98**, 184506 (2018).
- [36] M. Matusiak, E. M. Tunnicliffe, J. R. Cooper, Y. Matsushita, and I. R. Fisher, Evidence for a charge Kondo effect in $\text{Pb}_{1-x}\text{Ti}_x\text{Te}$ from measurements of thermoelectric power, *Phys. Rev. B* **80**, 220403 (2009).
- [37] G. E. McGuire, G. K. Schweitzer, and T. A. Carlson, Core electron binding energies in some group IIIA, VB, and VIB compounds, *Inorg. Chem.* **12**, 2450 (1973).
- [38] R. D. Zhong, J. A. Schneeloch, X. Y. Shi, Z. J. Xu, C. Zhang, J. M. Tranquada, Q. Li, and G. D. Gu, Optimizing the superconducting transition temperature and upper critical field of $\text{Sn}_{1-x}\text{In}_x\text{Te}$, *Phys. Rev. B* **88**, 020505 (2013).
- [39] S. Misra, B. Wiendlocha, J. Tobola, P. Levinský, J. Hejtmánek, S. Migot, J. Ghanbaja, A. Dauscher, B. Lenoir, and C. Candolfi, Influence of in-induced resonant level on the normal-state and superconducting properties of $\text{Sn}_{1.03}\text{Te}$, *Phys. Rev. B* **106**, 075205 (2022).
- [40] B. H. Freeland, J. J. Habeeb, and D. G. Tuck, Coordination compounds of indium. Part XXXIII. X-ray photoelectron spectroscopy of neutral and anionic indium halide species, *Can. J. Chem.* **55**, 1527 (1977).